Chemical Science

EDGE ARTICLE

View Article Online
View Journal | View Issue

Check for updates

Cite this: *Chem. Sci.*, 2020, **11**, 567

All publication charges for this article have been paid for by the Royal Society of Chemistry

Modulation of circularly polarized luminescence through excited-state symmetry breaking and interbranched exciton coupling in helical push–pull organic systems†

Kais Dhbaibi, [ah] Ludovic Favereau, *[a] Monika Srebro-Hooper, *[b] Cassandre Quinton, [a] Nicolas Vanthuyne, [c] Lorenzo Arrico, [d] Thierry Roisnel, [a] Bassem Jamoussi, [e] Cyril Poriel, [a] Clément Cabanetos, [f] Jochen Autschbach [g] and Jeanne Crassous *[a]

Received 16th October 2019
Accepted 19th November 2019

DOI: 10.1039/c9sc05231c

rsc.li/chemical-science

π-Helical push–pull dyes were prepared and their (chir)optical properties were investigated both experimentally and computationally. Specific fluorescent behaviour of bis-substituted system was observed with unprecedented solvent effect on the intensity of circularly polarized luminescence (CPL, dissymmetry factor decreasing from 10^{-2} to 10^{-3} with an increase in solvent polarity) that was linked to a change in symmetry of chiral excited state and suppression of interbranched exciton coupling. The results highlight the potential of CPL spectroscopy to study and provide a deeper understanding of electronic photophysical processes in chiral π-conjugated molecules.

Open Access Article. Published on 20 November 2019. Downloaded on 1/17/2025 4:01:46 PM.
This article is licensed under a Creative Commons Attribution-NonCommercial 3.0 Unported Licence.

Introduction

Circularly polarized (CP) luminescence (CPL) has attracted significant attention due to its potential applications in the fields of (chir)optoelectronics (stereoscopic displays, organic light-emitting diodes (OLED), optical information processing, *etc.*) as well as in bio-imaging and chiral sensing.[1] For a long time, lanthanide complexes have been the chiral molecular class of choice for studying CPL phenomena due to their (formally Laporte forbidden) f → f transitions, which provide them with large values (more than 1) luminescence dissymmetry factor $g_{lum} = 2(I_L - I_R)/(I_L + I_R)$.[2] In recent years, however, (small) chiral organic molecules have been gaining more and more interest as potential emitters thanks to their tuneable photophysical and chiroptical properties, and their relatively simple integration in optoelectronic devices such as CP-OLEDs, chiral photovoltaics and transistors.[2d,3] Indeed, this class of CPL emitters often exhibits superior luminescence quantum yields than lanthanide complexes owing to their electric dipole-allowed transitions. The involvement of such electronic transitions results however simultaneously in much lower g_{lum} values for organic systems, ranging from 10^{-4} to 10^{-2}, which hampers their use as emissive materials in chiroptoelectronic applications.[1d,f,g,4] Comprehensive synthetic guidelines for designing efficient chiral emitters are therefore currently needed to enable further developments in this field. Of particular importance here is identifying and understanding electronic factors that govern the g_{lum} at the molecular level, which still remains a crucial challenge for CPL dyes.[4b,c,5] The potential of CPL spectroscopy to investigate the chirality of the corresponding excited state is indeed largely unexplored in comparison with unpolarized fluorescence spectroscopy of achiral molecules.[6] For instance, solvent effects usually influence the emission and intensity wavelength (solvatochromism) through electronic interactions with the excited state.[7] For chiral emitters, such effects are rarely taken into consideration and associated g_{lum} is commonly defined only for one arbitrary solvent,[1f,4c] thus limiting the potential of CPL spectroscopy to provide unique information relating features of the chiral excited state to the intensity of polarized emission.[8] Consequently, a deep understanding of excited-state chirality is crucial from a fundamental point of view, as it may help to develop more efficient CPL

[a]*Univ Rennes, CNRS, ISCR – UMR 6226, ScanMAT – UMS 2001, F-35000 Rennes, France. E-mail: ludovic.favereau@univ-rennes1.fr; jeanne.crassous@univ-rennes1.fr*

[b]*Faculty of Chemistry, Jagiellonian University, Gronostajowa 2, 30-387 Krakow, Poland. E-mail: srebro@chemia.uj.edu.pl*

[c]*Aix Marseille University, CNRS, Centrale Marseille, iSm2, Marseille, France*

[d]*Dipartimento di Chimica e Chimica Industriale, University of Pisa, via Moruzzi 13, 56124, Pisa, Italy*

[e]*Department of Environmental Sciences, Faculty of Meteorology, Environment and Arid Land Agriculture, King Abdulaziz University, 21589 Jeddah, Saudi Arabia*

[f]*MOLTECH-Anjou, CNRS UMR 6200, University of Angers, 2 Bd Lavoisier, 49045 Angers, France*

[g]*Department of Chemistry, University at Buffalo, State University of New York, Buffalo, NY 14260, USA*

[h]*University of Gabès, Faculty of Science of Gabès, Zrig, 6072 Gabès, Tunisia*

† Electronic supplementary information (ESI) available. CCDC 1894823. For ESI and crystallographic data in CIF or other electronic format see DOI: 10.1039/c9sc05231c

Open Access Article. Published on 20 November 2019. Downloaded on 1/17/2025 4:01:46 PM.
This article is licensed under a Creative Commons Attribution-NonCommercial 3.0 Unported Licence.

emitters for CP-OLED, bio-imaging and chiral sensing where interactions between the chiral dye and its surroundings play a crucial role.

To investigate this hitherto unexplored aspect of CPL, we focus our attention on π-helical push–pull systems such as the newly synthesized mono-naphthalimide helicene **1** and the bis-naphthalimide helicene **2**, previously used in organic photovoltaic devices (Fig. 1).[3l] These are ideal candidates to explore innovative CPL-emitter designs based on intramolecular charge-transfer (ICT) transitions owing to the electron donor and electron acceptor abilities of the helicene and naphthalimide fragments, respectively.[9] As we report herein, the chiral multipolar acceptor (A)–π–donor (D) **1** and A–π–D–π–A **2** derivatives exhibit intense electronic circular dichroism (ECD) responses in the visible spectral region along with high fluorescence quantum yields and intense CPL signals, up to 80% and $g_{lum} = 10^{-2}$, respectively. Interestingly, while both compounds show similar solvatochromism, only **2** displays a modulation of CPL intensity with an increase in solvent polarity, showing the importance of the branching effect in such chiral push–pull dyes. The specific emission behaviour of **2** *vs.* **1** was rationalized based on both experimental and computational characterizations, and related mainly to a change in symmetry of the emitting S_1 state and suppression of exciton coupling between individual helicene → naphthalimide ICT transitions upon increasing the polarity of the environment.

Results and discussion

Synthesis and structural characterization

Enantiopure *P*-**1** and *P*-**2** were synthesized following the previously reported strategy[10] that involves a deprotection reaction of *P*-2,15-bis-(trimethylsilyl-ethynyl)[6]helicene (*P*-**H6(TMS)$_2$**) to obtain partially (*P*-**H6a**) and fully (*P*-**H6b**) unprotected ethynylhelicene derivatives (Scheme 1).[11] This statistical mixture was then directly engaged in a final Sonogashira coupling with

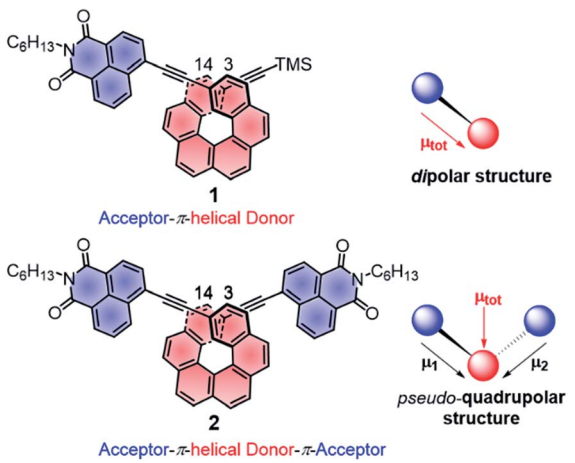

Fig. 1 Chemical structures of chiral A–π–D *P*-**1** and A–π–D–π–A *P*-**2** with schematic representations of the local and total permanent electric dipole moments μ. TMS: trimethylsilyl, C_6H_{13}: *n*-hexyl.

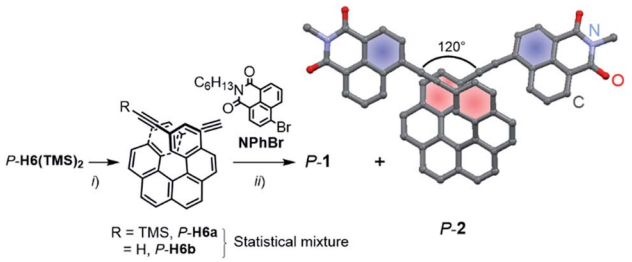

Scheme 1 Synthesis of enantiopure naphthalimide–helicene derivatives *P*-**1** and *P*-**2**. TMS: trimethylsilyl, C_6H_{13}: *n*-hexyl. Reaction conditions: (i) TBAF, $CHCl_3$; (ii) $Pd(PPh_3)_4$, CuI, Et_3N/toluene, 50 °C, **NPhBr**, 85% (*P*-**1**) and 90% (*P*-**2**). X-ray crystal structure of *P*-**2** (hexyl chains on the imide fragments have been omitted for clarity).

an excess of 6-bromo-2-hexyl-1*H*-benzoisoquinoline-1,3(2*H*)-dione (**NPhBr**),[3l] to afford *P*-**1** and *P*-**2** within the same reaction in 85–90% yield for both compounds (see ESI†). *M*-**1** and *M*-**2** were obtained in a similar way using *M*-2,15-bis-(trimethylsilyl-ethynyl)[6]helicene (*M*-**H6(TMS)$_2$**) as a starting material.

Characteristic signatures of both the [6]helicene and naphthalimide units were identified in the ^{1}H NMR spectra of **1** and **2**, which also showed the typical differences between C_1- and C_2-symmetric structures with two distinct signals (doublet of doublets) at 7.56 and 7.28 ppm assigned to H3 and H14 (Fig. 1) for **1** and only one signal (doublet) at 7.29 ppm for these protons in **2** (see also ESI†). Single crystals of *P*-**2** were obtained by slow diffusion of pentane vapours into CH_2Cl_2 solution. The compound crystallized in the non-centrosymmetric monoclinic $P2_1$ space group and displayed helicity (dihedral angle between the two terminal helicenic rings) of 37.77–47.91° (two molecules in the asymmetric unit), which is in the range of classical carbo[6]helicenes.[9d] Both naphthalimide fragments are oriented towards the helix, (*i.e.* with the aromatic ring not directly linked with the ethynyl bridge being in *cis* position with respect to the helicene) and show a dihedral angle of 7.2° with the corresponding terminal helicene phenyl ring. This should ensure a strong electronic communication between the two units (*vide infra*). The angle between each naphthalimide-ethynyl arms was estimated to be around 120° (Scheme 1) and allows to consider **2** as a *quasi*-quadrupolar A–π–D–π–A chiral compound.

UV-vis spectroscopy

UV-vis absorption spectra of **1** and **2** were recorded in CH_2Cl_2 and showed similar features but are noticeably different from those observed for their helicenic and naphthalimide precursors (Fig. 2a and S7 in the ESI†). Both compounds displayed three main bands with two higher-energy ones centered at *ca.* 300 and 360 nm that relate to absorption maxima of **H6(TMS)$_2$** and **NPhBr**, respectively, but are bathochromically shifted and more intense, and with an additional, strong, broad intensity at lower-energy, centered at 410 nm. Such modifications found in **1** and **2** compared to UV-vis spectra of precursors clearly reflect an extended π-electronic structure and push–pull effects within these helical naphthalimide systems (*vide infra*). Although no red-shift of the low-energy part of the spectrum was observed for

This journal is © The Royal Society of Chemistry 2020

Open Access Article. Published on 20 November 2019. Downloaded on 1/17/2025 4:01:46 PM.
This article is licensed under a Creative Commons Attribution-NonCommercial 3.0 Unported Licence.

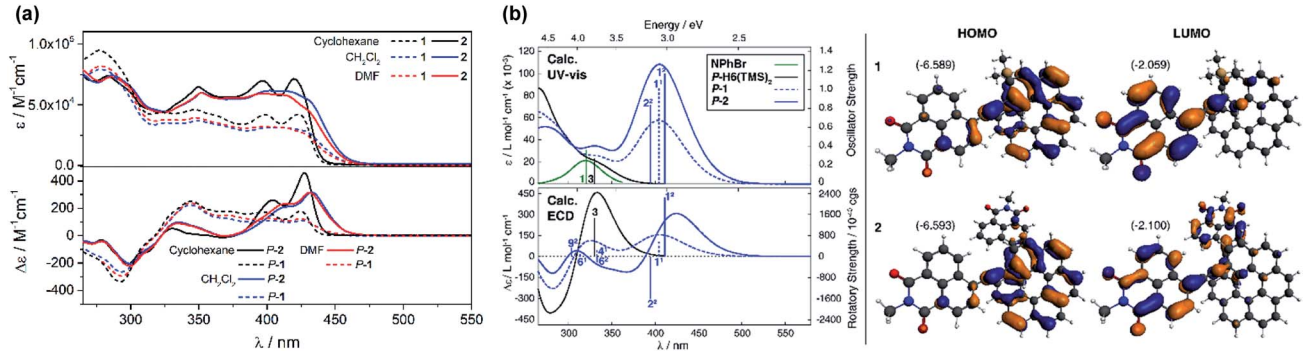

Fig. 2 (Panel a) Experimental UV-vis (top) and ECD (bottom) spectra of **1** (dashed lines) and **2** (solid lines) measured in cyclohexane (black), CH_2Cl_2 (blue) and DMF (red) at 298 K (~10^{-5} M). (Panel b) Comparison of the simulated UV-vis and ECD spectra of **1** and **2** with **H6(TMS)$_2$** and **NPhBr**. No spectral shift has been applied. Calculated excitation energies along with oscillator and rotatory strengths indicated as 'stick' spectra. Numbered excitations (N^1 for **1** and N^2 for **2**) correspond to those analyzed in detail. Isosurfaces (±0.03 au) of frontier MOs of **1** and **2**. Values listed in the parentheses are the corresponding orbital energies, in eV. See also ESI.†

2 *vs.* **1** (indicating lack of electronic conjugation through the whole helix in **2**) grafting two electron acceptor groups on the [6] helicene unit strongly affects absorption intensity in this spectral region leading to molar extinction coefficients for **2** twice as high as for **1** ($\varepsilon = 3.2 \times 10^4$ and $\varepsilon = 6.5 \times 10^4$ M^{-1} cm^{-1} at 410 nm for **1** and **2**, respectively, Fig. 2a). The absorption band at *ca.* 300 nm, assigned mainly to the helicene fragment (*vide infra*), appears slightly red-shifted by about 10 nm for **2** as compared to **1**, which confirms extension of helical π-electron system upon introduction of the second naphthalimide fragment. As shown in Fig. 2a and ESI (Fig. S8 and S9†), **1** and **2** exhibit almost no solvatochromism in their ground state. Only optical transitions between 370–450 nm display some slight shifts upon changing the solvent polarity, presumably due to their significant charge-transfer character (*vide infra*). However, these spectral changes are rather minor and exclusively observed in non-polar cyclohexane where both **1** and **2** exhibit a structured blue-shifted response with two distinct maxima, at 396 and 420 nm, equal in intensity ($\varepsilon = 4.1 \times 10^4$ and 7.2×10^4 M^{-1} cm^{-1} for **1** and **2**, respectively). This all indicates that naphthalimide–helicene derivatives **1** and **2** have moderate electronic dipole moments in their ground state.

Further characterizations of the electronic and photophysical properties of **1** and **2** were then obtained with the help of quantum-chemical calculations for truncated systems (with *n*-hexyl groups replaced by methyls) using (time-dependent) Kohn–Sham theory, (TD)KS = (TD)DFT.[12] All computational details along with the full set of theoretical results are provided in the ESI.† Conformational analyses (BP/SV(P)) performed for **1** and **2** revealed existence of two and three low-energy nearly isoenergetic conformers, respectively, that can be thus assumed to be present roughly in equal amounts at room temperature. These rotamer structures differ in the relative orientations of the naphthalimide group(s) and the helicene moiety (Fig. S18†) but demonstrate overall very similar electronic features with (i) the dipolar A–π–D and *pseudo*-quadrupolar A–π–D–π–A character for **1** and **2**, respectively, and (ii) efficient π-conjugation between electron acceptor naphthalimide group(s) and electron donor helicene moiety *via* the alkynyl bridge in both **1** and **2**. Indeed, calculated electronic dipole moment vectors in **1** and **2** are oriented as expected for the dipolar and *pseudo*-quadrupolar structures (Fig. S28 and S29†). Moreover, the frontier molecular orbitals (MOs) in **1** and **2** are consistent with the push–pull character of the dyes. Indeed, the occupied MOs span over the whole helicene fragment, the ethynyl bridges and partially also naphthalimide units, while the unoccupied ones are predominantly centered at the naphthalimide fragments but also delocalized over the adjacent helicene's rings *via* the alkynyl (Fig. 2b and ESI†). The simulated (BHLYP/SV(P), CH_2Cl_2 continuum solvent model), Boltzmann-averaged UV-vis absorption spectra (Fig. 2b) are in good agreement with the experimental ones (Fig. 2a). In particular, the appearance of the additional low-energy absorption bands in naphthalimide–helicene derivatives compared to their precursors **H6(TMS)$_2$** and **NPhBr** along with the significant increase in the absorption intensity observed for **2** *vs.* **1** are correctly reproduced by theory and linked to push–pull character of the dyes. In line with the A–π–D and A–π–D–π–A electronic structures of **1** and **2**, an MO-pair analysis of the dominant excitations calculated in the low-energy spectral regions assigns the additional absorption at 420 nm in **1** and **2** to mainly intramolecular charge-transfer π–π* excitations from the helicene core to the naphthalimide group(s). In the case of **1**, the band originates from the lowest-energy excitation no. 1^1 (calculated at 405 nm) that involves HOMO, HOMO−2 and LUMO (Fig. 2b and ESI†). For **2**, two excitations with sizeable oscillator strength were found in this spectral range, no. 1^2 and 2^2 calculated at 411 and 395 nm, respectively, that correspond to transitions from HOMO, HOMO−1, and HOMO−2 to LUMO and LUMO+1. Note that for both **1** and **2** occupied MOs involved in these excitations represent distinct π-orbitals of the alkynyl-helicene electron system with some contributions from the naphthalimide, while unoccupied MOs mainly extend over the naphthalimide-alkynyl group with LUMO and LUMO+1 in **2** representing in-phase and out-of-phase linear combinations of the naphthalimide substituents' LUMO. Accordingly, increase in the intensity of

Open Access Article. Published on 20 November 2019. Downloaded on 1/17/2025 4:01:46 PM.
This article is licensed under a Creative Commons Attribution-NonCommercial 3.0 Unported Licence.

the band for **2** is due to exciton-coupling (EC) interactions between these ICT states, similar to what we previously noticed for push–pull helicenic systems based on strongly electron acceptor tetracyanobutadienes.[13] Visible helicene → naphthalimide charge-transfer character can also be noticed for higher-energy excitations including those calculated around 300–330 nm with large contributions from the helicene-centered π–π* transitions (see ESI†). All this clearly supports the conclusions drawn from experimental optical observations.

Cyclic voltammetry

Electrochemical properties of **1** and **2** were examined *via* cyclic voltammetry measurements that resulted in potentials of *ca.* +1.4 V and −1.2 V *vs.* SCE for both compounds (Fig. S17 and Table S2†), assigned respectively to the oxidation of the helicene core and reduction of the naphthalimide unit(s).[14] While only one *quasi*-reversible reduction process was recorded for both systems, confirming a weak electronic interaction between the two naphthalimide units through the π-conjugated helix in **2**, bis-substituted naphthalimide–helicene derivative shows a slightly more positive oxidation potential than its mono-substituted analogue (ΔE_{Ox} = 80 mV), which is consistent with a decrease in the electronic density on the helicene core upon introduction of the second (electron deficient) naphthalimide group.

ECD spectroscopy

P- and *M*-**1** and *P*- and *M*-**2** compounds displayed electronic circular dichroism (ECD) with expected mirror-image relationships. Their ECD spectral signatures are strongly modified compared to those observed for *P*- and *M*-carbo[6]helicene derivatives (Fig. 2a).[15] For instance, *P*-**1** in CH_2Cl_2 solution exhibits an intense negative band ($\Delta\varepsilon$ = −290 M^{-1} cm^{-1}) at 293 nm that is 14 nm red-shifted compared to *P*-**H6(TMS)$_2$**, a large positive band between 320 and 450 nm with a maximum at 340 nm ($\Delta\varepsilon$ = +240 M^{-1} cm^{-1}), and three less intense peaks in the lowest-energy region ($\Delta\varepsilon$ = +150, +127, and +125 M^{-1} cm^{-1} at 370, 410, and 425 nm, respectively). *P*-**2** shows a similar high-energy negative ECD band at 300 nm ($\Delta\varepsilon$ = −220 M^{-1} cm^{-1}) that is only slightly less intense and red-shifted (by *ca.* 5 nm) compared to *P*-**1**. Its positive ECD signal between 320 and 370 nm becomes however much less intense and dips even slightly below zero ($\Delta\varepsilon$ = +90 M^{-1} cm^{-1} at 335 nm and −5 M^{-1} cm^{-1} at 370 nm *vs.* $\Delta\varepsilon$ = +230 M^{-1} cm^{-1} at 340 nm and +126 M^{-1} cm^{-1} at 370 nm, for *P*-**2** *vs.* *P*-**1**), while the region between 370 and 460 nm is now dominated by two very intense positive bands ($\Delta\varepsilon$ = +200 and +300 M^{-1} cm^{-1} at 410 and 430 nm, respectively), which are *ca.* 10 nm red-shifted in comparison to *P*-**1**. This significant increase in low-energy ECD intensity between *P*-**1** and *P*-**2** is reminiscent of what we reported for two other push–pull [6]helicene-based compounds bearing either diketopyrrolopyrrole (DPP) dyes[10] or tetracyanobutadiene (TCBD) electron withdrawing groups.[13] Their bis-substituted derivatives exhibit a chiral excitonic coupling originating from the helical arrangement of the two weakly interacting electronic dipoles of the π–π* excitations within a DPP dimer and of ICT helicene → TCBD excitations, respectively. In the present case, the naphthalimide group may act as both an achiral organic dye and an electron acceptor unit, affording a new example of chiral exciton coupling in helicenic systems that leads to one of the largest ECD signal at the molecular level in the visible region (*vide infra*).

Similarly to UV-vis absorption, changing the solvent polarity has rather minor effect on ECD spectra for both **1** and **2**, except for non-polar cyclohexane in which a 5 nm blue-shift of two lowest-energy bands along with their intensity increase were observed relative to peaks measured in more polar solvents (*e.g.* for *P*-**2**, $\Delta\varepsilon$ = +260 and +450 M^{-1} cm^{-1} at 404 and 426 nm, respectively, Fig. 2a, S10 and S11†). To provide a more quantitative characterization of the solvent effects for the examined systems, dissymmetry factors g_{abs} for all the studied solvents were then calculated and plotted (Fig. S12 and S13†). Their values range from 3.8×10^{-3} to 4.5×10^{-3} for *P*-**1** and from 7.0×10^{-3} to 9.5×10^{-3} for *P*-**2** at *ca.* 430 nm, which confirms the small impact of the polarity of the environment on the chiroptical ground-state responses of *P*-**1** and *P*-**2**. This is in line with the dipole moments calculated for both **1** (of 7–8 D) and **2** (of 6.5–7.5 D) that maintain the same spatial orientation and demonstrate only slight increase in magnitude with increase in the solvent polarity (Table S13 and Fig. S29†). Note also that among computationally examined solvents (cyclohexane, CH_2Cl_2, and DMF) the most pronounced change in the ground-state dipole moments of **1** and **2** upon increase in the solvent polarity is observed for cyclohexane *vs.* dichloromethane that may rationalize the most significant differences between spectra recorded in cyclohexane and those measured in remaining (more polar) solvents.

As shown in Fig. 2 and ESI,† the simulated (BHLYP/SV(P), CH_2Cl_2 continuum solvent model) ECD spectra of *P*-**1** and *P*-**2** agree well with the experimental results. In particular, the calculations correctly reproduced (i) the presence of positive ECD signal in the spectral region where the parent helicene absorbs, *i.e.* around 325 nm, for both *P*-**1** and *P*-**2**, with a decrease in the signal's intensity for the latter compound, and (ii) the appearance of low-energy intense positive ECD band along with its red-shift and strong increase in intensity for *P*-**2** *vs.* *P*-**1**. As expected and aforementioned above, the former band indeed originates from the predominantly helicene-centered π–π* excitations (no. 4^1 computed at 333 nm and 6^1 at 314 nm for **1** and no. 9^2 at 304 nm for **2** in Fig. 2b, see also ESI†) that involve, however, also ICT transitions from the helicene's π-electron system to the naphthalimide group(s), whereas the low-energy band is attributed to intense lowest-energy excitation (no. 1^1 (405 nm) and 1^2 (411 nm)) of purely helicene → naphthalimide ICT character. In the case of **2**, this first excitation is accompanied by analogous helicene → naphthalimide ICT excitation no. 2^2 (395 nm) that reveals similar energy along with comparable, although opposite-sign, rotatory strength value. In consequence, the appearance of a strong bisignate pair of bands in the low-energy part of the computed ECD spectrum of **2** is observed. The bisignate signature and significant enhancement of the long-wavelength ECD intensity for **2** *vs.* **1** along with the donor → acceptor ICT character of underlying excitations

 This journal is © The Royal Society of Chemistry 2020

Open Access Article. Published on 20 November 2019. Downloaded on 1/17/2025 4:01:46 PM.
This article is licensed under a Creative Commons Attribution-NonCommercial 3.0 Unported Licence.

clearly resemble the case of helicene–TCBD derivatives, and based on its analysis presented in ref. 13, the ECD-intense low-energy excitations of **2**, 1^2 and 2^2, can also be treated as the exciton couplet arising from coupling between transitions from helicene's π-orbitals to the π*-orbital localized at either one of the naphthalimide groups. The effect is clearly enhanced with respect to TCBD-functionalized helicenes which may be due to a more efficient π-conjugation between electron acceptor substituents and helicene moiety occurring in **2** promoted by highly conjugated and aromatic structure of the naphthalimide dye. The intensity of the band originating from the negative couplet component for *P*-**2** appears to be additionally increased by a presence of excitation no. 6^2 (333 nm) that also reveals sizable negative rotatory strength value, which may be responsible for the substantial overestimation of the calculated ECD response at around 350 nm for this compound compared to the experimental results. Furthermore, it is worth noting that the experimental intensity of this band (see Fig. S11†) seems to decrease with the polarity of the solvent which may indicate suppression of exciton-coupling interactions between the ICT states in **2** in polar solvents.

Unpolarized luminescence and excited-state symmetry breaking

Fluorescence responses of **1** and **2** appear rather independent on the number of naphthalimide electron acceptor units, showing only a slight blue-shift of the spectra for **2** *vs.* **1**, and, contrary to the UV-vis absorption and ECD, display significant positive solvatochromism with typical (and similar for both compounds) red-shift of the emission spectra with an increase in the solvent polarity (Table 1 and Fig. S14†). For example, and as illustrated in Fig. 3a for **2**, the structured emission in cyclohexane with two distinct bands at 436 and 462 nm becomes less structured and slightly red-shifted in toluene (λ_{max} = 459 nm), while further gradual increase in the polarity of the solvent results in a broad emission profile with its maximum located from 496 nm in THF to 565 nm in DMF. Such pronounced red-shifts of fluorescence spectra and no obvious shift of the absorption in various solvents lead to a significant increase in the Stokes shifts with increasing solvent polarity for **1** and **2** that is consistent with the formation of ICT-type excited state with a much larger dipole moment than in the ground state for both compounds. As presented in Fig. 3b, the solvent-dependent fluorescence behaviour of **1** and **2** overall follows well the Lippert–Mataga relationship between Stokes shift $\Delta\nu$ (in cm^{-1}) and solvent orientational polarizability Δf values (eqn (1) and (2)):[6a,16]

$$\Delta\nu = \nu_{ab} - \nu_{em} = \frac{2(\Delta\mu_{eg})^2}{hca_0^3}\Delta f + \text{constant} \quad (1)$$

$$\Delta f = f(\varepsilon) - f(n^2) \approx \frac{\varepsilon - 1}{2\varepsilon + 1} - \frac{n^2 - 1}{2n^2 + 1} \quad (2)$$

where $\Delta\mu_{eg}$ is the difference between dipole moments of the excited (μ_e) and ground (μ_g) states ($\Delta\mu_{eg} = \mu_e - \mu_g$, with its magnitude given in D); h, the Planck constant (=6.6256×10^{-27} erg s); c, the light velocity (=2.9979×10^{10} cm s^{-1}); a_0, the radius of the solute's Onsager cavity (in Å); ε and n the dielectric constant and refractive index of the solvent, respectively.

These results indicate that the observed spectral shifts in solution are determined by dipole–dipole type interactions between the helical fluorophore and solvent molecules rather than by specific solute–solvent interactions such as hydrogen bonding. More interesting, the plots show nearly identical behaviour with large and similar slope values for both **1** and **2** suggesting that fluorescence in these compounds stems from an excited state of essentially the same electronic nature and is accompanied by large values of the effective dipole moment change $\Delta\mu_{eg}$ (Table S12†). Such large slopes appear to reflect relatively small Stokes shifts of **1** and **2** in cyclohexane and toluene, which, along with the structured luminescence profile and the symmetry observed between the absorption and emission spectra, suggests a smaller reorganization before emission in non-polar solvents (*i.e.* weaker charge-transfer character of S_1 excited states) for these systems. Further luminescence characterizations, including fluorescence quantum yields (ϕ_{fluo}) and lifetime decays measurements, also confirm a similar photophysical behaviour of **1** and **2** (Table 1). Namely, both compounds display moderate to intense emission efficiencies in the different solvents with ϕ_{fluo} up to 85% and 75% for **1** and

Table 1 Photophysical data for **1** and **2** in selected solvents

	D–π–A **1**						A–π–D–π–A **2**					
Solvent	λ_{abs} (nm)	λ_{em} (nm)	$\Delta\nu^a$ (cm^{-1})	$\phi_{fluo}{}^b$ (%)	$\tau_{fluo}{}^c$ (ns)	$\lvert g_{lum}\rvert$ ($\times 10^{-3}$)	λ_{abs} (nm)	λ_{em} (nm)	$\Delta\nu^a$ (cm^{-1})	$\phi_{fluo}{}^b$ (%)	$)\tau_{Fluo}{}^c$ (ns]	$\lvert g_{lum}\rvert$ ($\times 10^{-3}$)
CyH	420	436	870	70	2.1	3.2	420	436	1030	45	2.4 (91%)	9.5
Tol	428	457	1480	85	3.4	2.4	430	453	1180	65	2.8	6.5
THF	424	503	3700	80	4.4	2.0	423	497	3520	75	4.3	4.0
$CHCl_3$	431	509	3560	80	4.0	2.0	432	503	3270	70	4.2	4.0
CH_2Cl_2	427	527	4440	75	4.7	1.8	427	520	4000	70	4.3 (96%)	3.1
Acetone	424	548	5340	65	5.7	1.8	429	539	4790	60	5.7	2.8
DMF	427	576	6060	55	6.2	1.8	433	562	5450	55	6.3 (97%)	2.5

[a] Stokes shift. [b] Absolute quantum yield (error ± 10%), measured using an integrating sphere. [c] Fluorescence lifetime (error ± 5%), only the main component decay is given (weight in parenthesis).

Open Access Article. Published on 20 November 2019. Downloaded on 1/17/2025 4:01:46 PM.
This article is licensed under a Creative Commons Attribution-NonCommercial 3.0 Unported Licence.

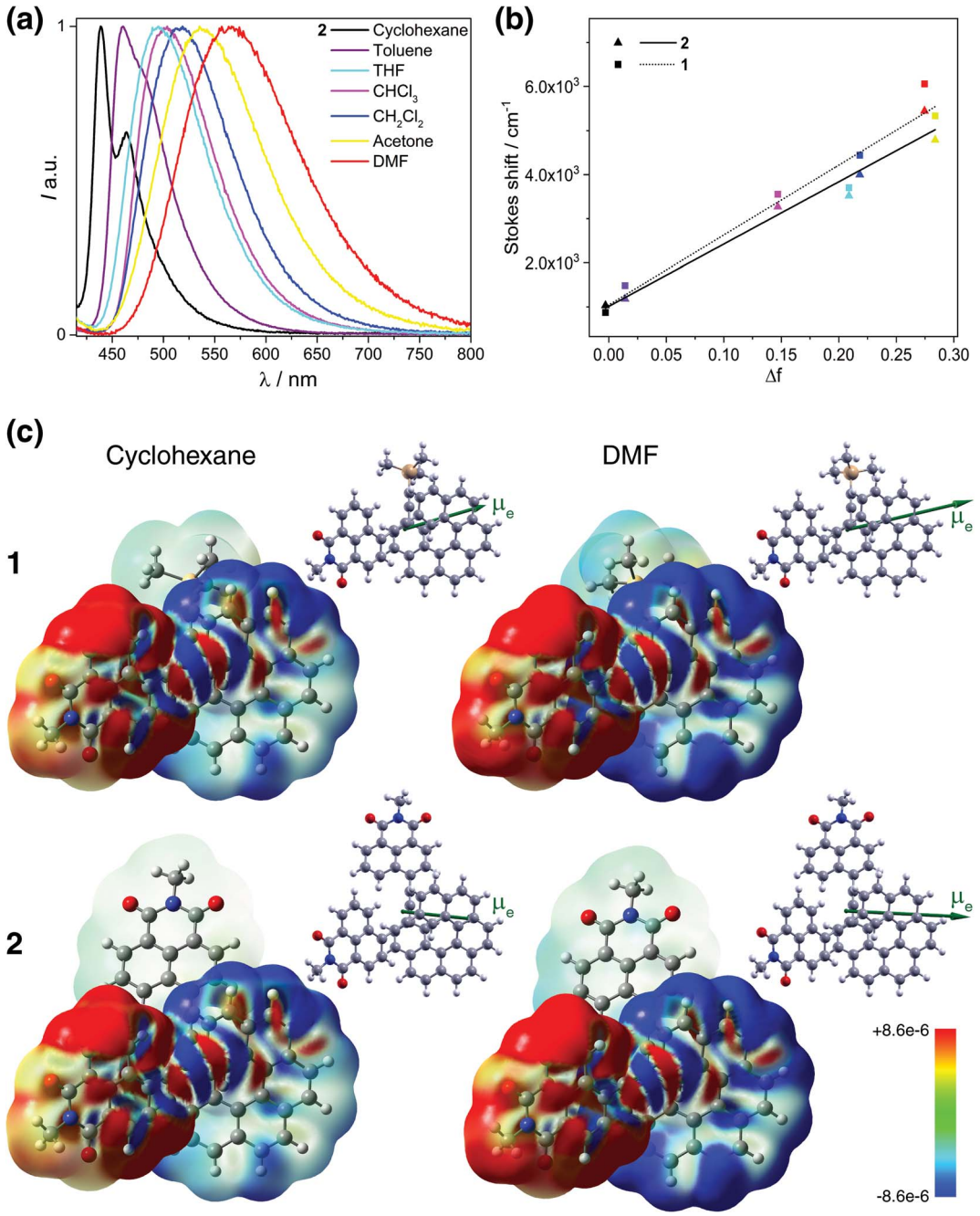

Fig. 3 (Panel a) Emission of **2** in cyclohexane (black), toluene (purple), THF (sky blue), $CHCl_3$ (pink), CH_2Cl_2 (blue), acetone (yellow), and DMF (red) at 298 K ($\sim 10^{-5}$ M). (Panel b) Lippert–Mataga plots for **1** (dotted line) and **2** (solid line) (see also Table S12†). (Panel c) Difference density between the S_0 ground state and S_1 excited state, $\Delta\rho = \rho_g - \rho_e$, color-mapped on ρ_g (± 0.0003 au) for **1** and **2** in cyclohexane and DMF. Alongside, the corresponding S_1 excited-state dipole moment vectors (with origin located at the center of nuclear charge, scaled by a factor of 0.5, pointing from the negative to the positive pole of the dipole) are shown. TDDFT BHLYP/SV(P) continuum solvent model calculations. See also ESI.†

2, respectively. Fluorescence lifetimes of **1** and **2** increase from *ca.* 2.5 ns in cyclohexane to 6.3 ns in DMF, which also evidence the impact of polarity on the charge-transfer excited-state dynamics.

All these experimental observations are well corroborated by TDDFT emission modeling employing state-specific solvation for cyclohexane ($\varepsilon = 2.0$), CH_2Cl_2 ($\varepsilon = 8.9$), and DMF ($\varepsilon = 37.2$) (see Computational details in the ESI†). The calculations nicely reproduced the solvent-dependent fluorescence behaviour of **1** and **2** with theoretical emission maxima very close to the experimental ones (Tables S10 and S11†). Values of the computed S_1 electronic dipole moments visibly increase with the solvent polarity, from *ca.* 16 and 13 D in cyclohexane to 24 and 21 D in DMF for **1** and **2**, respectively, and are strongly enhanced (*ca.* 2–3 times) compared to those in S_0, confirming that the excited state of these compounds is more polar than the

 This journal is © The Royal Society of Chemistry 2020

Open Access Article. Published on 20 November 2019. Downloaded on 1/17/2025 4:01:46 PM.
This article is licensed under a Creative Commons Attribution-NonCommercial 3.0 Unported Licence.

ground state (Table S13, Fig. S29 and S30†). More importantly, a significant change in the orientation of μ_e vector compared to that of μ_g is observed for **2** toward that observed for **1** and typical for dipolar structure (Fig. 3a, S29 and S30†). Additionally, the magnitude of the effective dipole moment change $\Delta\mu_{eg}$ is large and almost the same for both compounds (Table S14†). The calculations also enabled to confirm fundamentally identical nature of the emitting excited state in **1** and **2**. In Fig. 3c, the difference densities between the ground state and the excited state for **1** and **2** are presented with their negative (red)/positive (blue) values corresponding to outflow/inflow of electron density accompanying $S_1 \rightarrow S_0$ fluorescence transition (see also Fig. S32†). It is clearly seen that S_1 for both **1** and **2** exhibits the same intramolecular naphthalimide → helicene CT characteristics with involvement of only one naphthalimide unit in the case of **2** due to the excited-state symmetry-breaking effect (*vide infra*).[17] Such localization is consistent with the observed 'dipolar-like' orientation of μ_e vector and rationalizes similar photophysical behaviour of both naphthalimide–helicenes. The difference density plots also reveals noticeable increase in the charge-transfer character of S_1 excited states (more electron density transferred from naphthalimide group to helicene moiety) for **1** and **2** with the increase in the polarity of the solvent correlating well with the corresponding rise of μ_e values and higher stabilization of the excited state by polar solvents reflected in the larger red-shift of fluorescence spectra in such environments. The analysis of $S_1 \rightarrow S_0$ emission in terms of individual MO pairs (Fig. S31 and Table S15†) shows that the process mainly corresponds to LUMO → HOMO transition with LUMO localized predominantly on the naphthalimide-alkynyl group and HOMO spanning over the helicene-alkynyl fragment and partially naphthalimide unit. While isosurface of LUMO hardly changes with the polarity of the solvent, for HOMO less/more electron density is observed on naphthalimide/helicene when going from cyclohexane to DMF, in agreement with the increase in the CT character of S_1 for **1** and **2** in more polar environment.

Summarizing, unpolarized luminescence measurements and calculations for mono- and bis-substituted naphthalimide–helicene derivatives **1** and **2** reveal a similar evolution of their first excited state with the solvent polarity, even though the latter may be viewed in its ground state as *pseudo*-quadrupolar A–π–D–π–A structure with a slightly smaller resultant electronic dipole moment than in **1**. Such behaviour has been reported for numerous multibranched achiral push–pull molecules,[17] and rationalized in terms of a symmetry-breaking in excited state due to structural fluctuations *via* vibrational relaxation and/or solvation effects. The reported computations demonstrate essentially the same character of S_1 excited state for **2** in both non-polar and polar solvents (and also in gas-phase) indicating that the observed localization of the excitation is predominantly induced by nuclear relaxation that involves mainly planarization of the naphthalimide units with respect to the corresponding terminal helicene phenyl ring (leading consequently to increase in naphthalimide–helicene π-conjugation) upon excited-state geometry optimization (Fig. S26†). Note that similar excited-state localization for an A–π–D–π–A-type system was reported and described in terms of a Frenkel exciton model for example in ref. 17*a*. Note also that Vauthey *et al.* have recently been able to directly visualize such excited-state symmetry-breaking process using ultra-fast time-resolved infrared spectroscopy, thus providing fundamental understanding of this phenomenon and opening new perspectives for multipolar π-conjugated systems in optoelectronic applications and photochemistry.[17d,e,18]

CPL and interbranched excition coupling

To further investigate the impact of solvatochromism on the chiral excited states of **1** and **2**, the corresponding CPL spectra were recorded in the same set of solvents used in the unpolarized luminescence study (Fig. 4, S15 and S16†). As can be seen, both compounds display intense, mirror-image CPL signals for *P* and *M* enantiomers with similar red-shifts upon increasing the polarity of the solvent, in agreement with unpolarized emission. Interestingly, while *P*-**1** exhibits almost constant CPL intensity in all solvents ($g_{lum} \sim 2 \times 10^{-3}$), *P*-**2** shows an unexpected three-fold decrease of intensity when going from non-polar to polar environment (Fig. 5 and Table 1). Namely, the intense structured CPL spectrum for *P*-**2** in cyclohexane ($g_{lum} = 9.5 \times 10^{-3}$) becomes broader in toluene ($g_{lum} = 6.5 \times 10^{-3}$), and unstructured and weakened in THF and $CHCl_3$ ($g_{lum} = 4.0 \times 10^{-3}$). For more polar solvents (CH_2Cl_2, acetone, and DMF) a further decrease in intensity of the *P*-**2** CPL signal (with g_{lum} values of *ca.* 3.0×10^{-3}) was observed.

The effect of the solvation on CPL intensity is also visible in the computed results that show almost constant rotatory strength *R* and the corresponding g_{lum} values for $S_1 \rightarrow S_0$ fluorescence transition in different solvents for **1**, and their noticeable (although clearly underestimated comparing to the experiment) increase when changing the polarity of the solvent from CH_2Cl_2 and DMF to cyclohexane for **2** (Tables S10 and

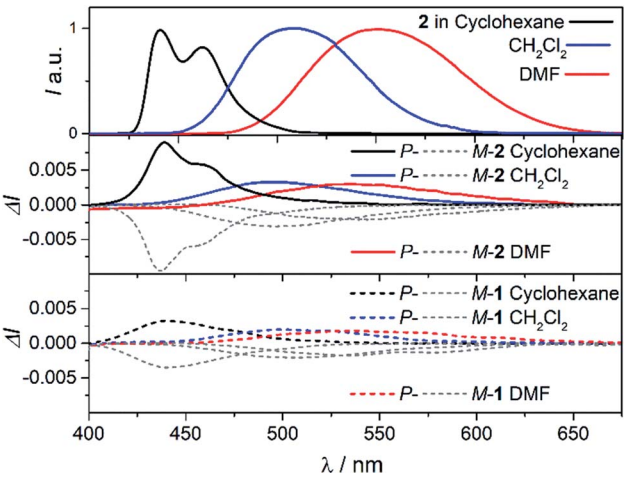

Fig. 4 CPL spectra of **2** (middle panel) and **1** (bottom panel) in cyclohexane (black), CH_2Cl_2 (blue), and DMF (red) at 298 K (~10^{-5} M). For a comparison, fluorescence spectra of **2** are presented in the top panel (the corresponding spectra for **1** are not shown as they are similar to those for **2**). See ESI† for a full set of recorded spectra.

Open Access Article. Published on 20 November 2019. Downloaded on 1/17/2025 4:01:46 PM.
This article is licensed under a Creative Commons Attribution-NonCommercial 3.0 Unported Licence.

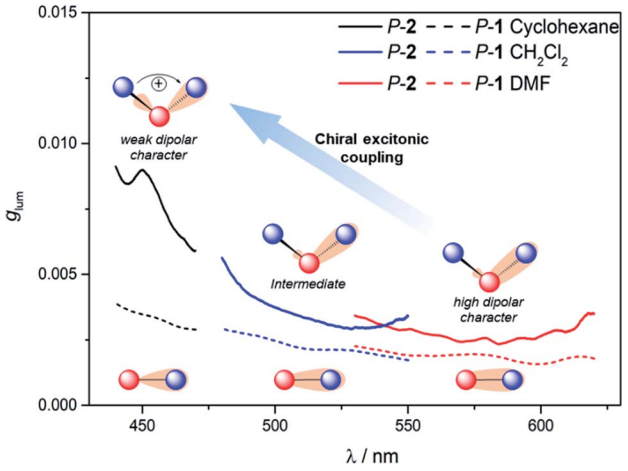

Fig. 5 Emission dissymmetry factors g_{lum} of *P*-**1** (dashed lines) and *P*-**2** (solid lines) in cyclohexane (black), CH_2Cl_2 (blue), and DMF (red) at 298 K (~10^{-5} M) along with illustration of the effects underlying the observed trends.

S11†). Keeping in mind that R is a function of the magnitudes of the underlying electric d and magnetic m transition dipole moments and the angle θ between their vectors, this enhancement can be traced back to an increase in the value of m and a more beneficial orientation factor observed in **2** for cyclohexane *vs.* more polar solvents (Table S15 and Fig. S33†). This solvent-dependent modulation of m and θ along with the chiral exciton coupling between individual helicene → naphthalimide ICT transitions established in the low-energy region of the UV-vis and ECD spectra for **2** (with $S_0 \rightarrow S_1$ and $S_0 \rightarrow S_2$ constituting the exciton couplet) indicate that its unprecedented for organic CPL emitters behaviour can also be linked to the corresponding coupling in the excited state with the resulting lower-energy couplet's component (emitting S_1 state) undergoing localization on one naphthalimide branch due to nuclear relaxation. This seems to be further supported by overall strong enhancement of the CPL intensity for **2** *vs.* **1** visible in the experiment following similar trends in the UV-vis and ECD signals. In the presence of an intense reaction field imposed by the polar solvents the electrostatic interaction between electric transition dipoles (each connected with either one of the electron acceptor unit) is suppressed,[17i] affecting magnetic transition dipoles and their relative orientations, and, as a consequence, a decrease in the CPL intensity is observed.

Finally, it is thus worth emphasizing that **2** exhibits in cyclohexane one of the highest g_{lum} values reported to date for (small) organic molecules in solution,[1f,4c,19] which highlights the benefits of chiral exciton coupling strategy to enhance the chiroptical properties of helicene-based dyes.

Conclusions

We have synthesized chiral push–pull A–π–D and A–π–D–π–A organic CPL emitters based on the functionalization of enantiopure [6]helicene with naphthalimide chromophores. Unpolarized and polarized characterizations revealed much more intense ECD signal ($\Delta\varepsilon$ = +456 M^{-1} cm^{-1} at 430 nm) and CPL activity with g_{lum} up to 10^{-2} for the bis-substituted *P*-**2** than for its mono-substituted analogue *P*-**1** ($\Delta\varepsilon$ = +179 M^{-1} cm^{-1} at 430 nm, $g_{lum} < 3 \times 10^{-3}$), arising from an intramolecular chiral exciton coupling effect. Being highly luminescent (ϕ_{fluo} up to 0.85), these chiral emitters display also significant solvatochromism, which strongly impacts the intensity of polarized emission for **2**, with a pronounced decrease of g_{lum} when going from non-polar cyclohexane ($g_{lum} = 10^{-2}$) to polar dimethylformamide solvent ($g_{lum} = 3 \times 10^{-3}$), despite the overall similar fluorescent behaviour of both **1** and **2**. This was associated with a symmetry breaking of the emitting S_1 state in **2** adopting fundamentally identical nature as in **1** and suppression of exciton coupling between individual helicene → naphthalimide ICT transitions upon increasing the solvent polarity. These unprecedented results highlight the potential of CPL spectroscopy to investigate and characterize electronic features of luminescent states in organic chiral π-conjugated systems and to provide a deeper understanding of the underlying photophysical effects that may open new directions for designing novel efficient CPL emitters.

Conflicts of interest

There are no conflicts of interest to declare.

Acknowledgements

We acknowledge the Ministère de l'Education Nationale, de la Recherche et de la Technologie, the Centre National de la Recherche Scientifique (CNRS). K. D. is grateful for financial support from the University of Gabès, the University of Rennes 1, and Campus France. J. A. thanks the National Science Foundation (CHE-1855470) for financial support and the Center for Computational Research (CCR) at the University at Buffalo for computational resources. C. C. thanks the region pays de la loire for the "SAMOA" project. The PRISM core facility (Biogenouest©, UMS Biosit, Université de Rennes 1 – Campus de Villejean – 35043 RENNES Cedex, FRANCE) is acknowledged for the NMR characterizations and ECD measurements. Dr Y. Molard (ISCR, Rennes) is thanked for luminescence quantum yield measurements and Dr P.-A. Bouit (ISCR, Rennes) for fruitful discussions. Prof. L. Di Bari and Dr M. Górecki are warmly thanked for their assistance in CPL measurements.

References

1 (*a*) F. S. Richardson and J. P. Riehl, *Chem. Rev.*, 1977, **77**, 773–792; (*b*) J. P. Riehl and F. S. Richardson, *Chem. Rev.*, 1986, **86**, 1–16; (*c*) *Chirality at the Nanoscale, Nanoparticles, Surfaces, Materials and more*, ed. D. Amabilino, Wiley-VCH, 2009; (*d*) J. Kumar, T. Nakashima and T. Kawai, *J. Phys. Chem. Lett.*, 2015, **6**, 3445–3452; (*e*) B. Kunnen, C. Macdonald, A. Doronin, S. Jacques, M. Eccles and I. Meglinski, *J. Biophotonics*, 2015, **8**, 317–323; (*f*) E. M. Sánchez-Carnerero, A. R. Agarrabeitia, F. Moreno, B. L. Maroto, G. Muller, M. J. Ortiz and S. de la Moya, *Chem.–Eur. J.*, 2015, **21**,

 This journal is © The Royal Society of Chemistry 2020

Open Access Article. Published on 20 November 2019. Downloaded on 1/17/2025 4:01:46 PM.
This article is licensed under a Creative Commons Attribution-NonCommercial 3.0 Unported Licence.

13488–13500; (*g*) J. Han, S. Guo, H. Lu, S. Liu, Q. Zhao and W. Huang, *Adv. Opt. Mater.*, 2018, **6**, 1800538.

2 (*a*) F. Zinna and L. Di Bari, *Chirality*, 2015, **27**, 1–13; (*b*) S. Shuvaev, E. A. Suturina, K. Mason and D. Parker, *Chem. Sci.*, 2018, **9**, 2996–3003; (*c*) S. Shuvaev, M. A. Fox and D. Parker, *Angew. Chem., Int. Ed.*, 2018, **57**, 7488–7492; (*d*) F. Zinna, M. Pasini, F. Galeotti, C. Botta, L. Di Bari and U. Giovanella, *Adv. Funct. Mater.*, 2017, **27**, 1603719.

3 (*a*) M. Li, S. H. Li, D. Zhang, M. Cai, L. Duan, M. K. Fung and C. F. Chen, *Angew. Chem., Int. Ed. Engl.*, 2018, **57**, 2889–2893; (*b*) J. Han, S. Guo, J. Wang, L. Wei, Y. Zhuang, S. Liu, Q. Zhao, X. Zhang and W. Huang, *Adv. Opt. Mater.*, 2017, **5**, 1700359; (*c*) T.-Y. Li, Y.-M. Jing, X. Liu, Y. Zhao, L. Shi, Z. Tang, Y.-X. Zheng and J.-L. Zuo, *Sci. Rep.*, 2015, **5**, 14912; (*d*) J. R. Brandt, X. Wang, Y. Yang, A. J. Campbell and M. J. Fuchter, *J. Am. Chem. Soc.*, 2016, **138**, 9743–9746; (*e*) S. Feuillastre, M. Pauton, L. Gao, A. Desmarchelier, A. J. Riives, D. Prim, D. Tondelier, B. Geffroy, G. Muller, G. Clavier and G. Pieters, *J. Am. Chem. Soc.*, 2016, **138**, 3990–3993; (*f*) M. Schulz, M. Mack, O. Kolloge, A. Lutzen and M. Schiek, *Phys. Chem. Chem. Phys.*, 2017, **19**, 6996–7008; (*g*) J. Gilot, R. Abbel, G. Lakhwani, E. W. Meijer, A. P. H. J. Schenning and S. C. J. Meskers, *Adv. Mater.*, 2010, **22**, E131–E134; (*h*) X. Shang, I. Song, H. Ohtsu, Y. H. Lee, T. Zhao, T. Kojima, J. H. Jung, M. Kawano and J. H. Oh, *Adv. Mater.*, 2017, **29**, 1605828; (*i*) Y. Yang, B. Rice, X. Shi, J. R. Brandt, R. Correa da Costa, G. J. Hedley, D. M. Smilgies, J. M. Frost, I. D. W. Samuel, A. Otero-de-la-Roza, E. R. Johnson, K. E. Jelfs, J. Nelson, A. J. Campbell and M. J. Fuchter, *ACS Nano*, 2017, **11**, 8329–8338; (*j*) Y. Yang, R. C. da Costa, M. J. Fuchter and A. J. Campbell, *Nat. Photonics*, 2013, **7**, 634–638; (*k*) F. Song, Z. Xu, Q. Zhang, Z. Zhao, H. Zhang, W. Zhao, Z. Qiu, C. Qi, H. Zhang, H. H. Y. Sung, I. D. Williams, J. W. Y. Lam, Z. Zhao, A. Qin, D. Ma and B. Z. Tang, *Adv. Funct. Mater.*, 2018, **28**, 1800051; (*l*) P. Josse, L. Favereau, C. Shen, S. Dabos-Seignon, P. Blanchard, C. Cabanetos and J. Crassous, *Chem.–Eur. J.*, 2017, **23**, 6277–6281; (*m*) N. Y. Kim, J. Kyhm, H. Han, S. J. Kim, J. Ahn, D. K. Hwang, H. W. Jang, B.-K. Ju and J. A. Lim, *Adv. Funct. Mater.*, 2019, **29**, 1808668; (*n*) M. Schulz, F. Balzer, D. Scheunemann, O. Arteaga, A. Lützen, S. C. J. Meskers and M. Schiek, *Adv. Funct. Mater.*, 2019, **29**, 1900684; (*o*) F. Zinna, U. Giovanella and L. D. Bari, *Adv. Mater.*, 2015, **27**, 1791–1795.

4 (*a*) H. Maeda and Y. Bando, *Pure Appl. Chem.*, 2013, **85**, 1967; (*b*) N. Chen and B. Yan, *Molecules*, 2018, **23**, 3376; (*c*) H. Tanaka, Y. Inoue and T. Mori, *ChemPhotoChem*, 2018, **2**, 386–402.

5 H. Tanaka, M. Ikenosako, Y. Kato, M. Fujiki, Y. Inoue and T. Mori, *Commun. Chem.*, 2018, **1**, 38.

6 (*a*) J. R. Lakowicz, *Principles of Fluorescence Spectroscopy*, Springer, New York, 2006; (*b*) B. Valeur, *Molecular Fluorescence: Principles and Applications*, Wiley-VCH, Weinheim, 2001.

7 (*a*) P. Suppan and N. Ghoneim, *Solvatochromism*, The Royal Society of Chemistry, Cambridge, 1997; (*b*) C. Reichardt, *Solvent and solvent effects in organic chemistry*, Wiley-VCH, Weinheim, 3rd edn, 2002; (*c*) A. Marini, A. Muñoz-Losa, A. Biancardi and B. Mennucci, *J. Phys. Chem. B*, 2010, **114**, 17128–17135.

8 (*a*) Rare examples where CPL was recorded in different solvents without intense solvatochromism effect on intensity of polarization emission effects; (*b*) H. Nishimura, K. Tanaka, Y. Morisaki, Y. Chujo, A. Wakamiya and Y. Murata, *J. Org. Chem.*, 2017, **82**, 5242–5249; (*c*) S. Nakanishi, N. Hara, N. Kuroda, N. Tajima, M. Fujiki and Y. Imai, *Org. Biomol. Chem.*, 2018, **16**, 1093–1100.

9 (*a*) P. Gopikrishna, N. Meher and P. K. Iyer, *ACS Appl. Mater. Interfaces*, 2018, **10**, 12081–12111; (*b*) Y. Yoshida, Y. Nakamura, H. Kishida, H. Hayama, Y. Nakano, H. Yamochi and G. Saito, *CrystEngComm*, 2017, **19**, 3626–3632; (*c*) T. Kogiso, K. Yamamoto, H. Suemune and K. Usui, *Org. Biomol. Chem.*, 2012, **10**, 2934–2936; (*d*) Y. S. C.-F. Chen, *Helicenes Chemistry: From Synthesis to Applications*, Springer, Berlin, 2017.

10 K. Dhbaibi, L. Favereau, M. Srebro-Hooper, M. Jean, N. Vanthuyne, F. Zinna, B. Jamoussi, L. Di Bari, J. Autschbach and J. Crassous, *Chem. Sci.*, 2018, **9**, 735–742.

11 E. Anger, M. Srebro, N. Vanthuyne, L. Toupet, S. Rigaut, C. Roussel, J. Autschbach, J. Crassous and R. Réau, *J. Am. Chem. Soc.*, 2012, **134**, 15628–15631.

12 (*a*) J. Autschbach, *Chirality*, 2009, **21**, E116–E152; (*b*) M. Srebro-Hooper and J. Autschbach, *Annu. Rev. Phys. Chem.*, 2017, **68**, 399–420.

13 R. Bouvier, R. Durand, L. Favereau, M. Srebro-Hooper, V. Dorcet, T. Roisnel, N. Vanthuyne, Y. Vesga, J. Donnelly, F. Hernandez, J. Autschbach, Y. Trolez and J. Crassous, *Chem.–Eur. J.*, 2018, **24**, 14484–14494.

14 S. M. McAfee, J. R. Cann, P. Josse, P. Blanchard, C. Cabanetos and G. C. Welch, *ACS Sustainable Chem. Eng.*, 2016, **4**, 3504–3517.

15 (*a*) Y. Nakai, T. Mori and Y. Inoue, *J. Phys. Chem. A*, 2012, **116**, 7372–7385; (*b*) Y. Nakai, T. Mori and Y. Inoue, *J. Phys. Chem. A*, 2013, **117**, 83–93.

16 J. Zhang, C. Zhao, H. Liu, Y. Lv, R. Liu, S. Zhang, H. Chen, G. Zhang and Z. Tian, *J. Phys. Chem. C*, 2015, **119**, 2761–2769.

17 (*a*) C. Katan, F. Terenziani, O. Mongin, M. H. V. Werts, L. Porrès, T. Pons, J. Mertz, S. Tretiak and M. Blanchard-Desce, *J. Phys. Chem. A*, 2005, **109**, 3024–3037; (*b*) H. Y. Woo, B. Liu, B. Kohler, D. Korystov, A. Mikhailovsky and G. C. Bazan, *J. Am. Chem. Soc.*, 2005, **127**, 14721–14729; (*c*) U. Megerle, F. Selmaier, C. Lambert, E. Riedle and S. Lochbrunner, *Phys. Chem. Chem. Phys.*, 2008, **10**, 6245–6251; (*d*) B. Dereka, A. Rosspeintner, M. Krzeszewski, D. T. Gryko and E. Vauthey, *Angew. Chem., Int. Ed.*, 2016, **55**, 15624–15628; (*e*) B. Dereka, A. Rosspeintner, Z. Li, R. Liska and E. Vauthey, *J. Am. Chem. Soc.*, 2016, **138**, 4643–4649; (*f*) B. Dereka, M. Koch and E. Vauthey, *Acc. Chem. Res.*, 2017, **50**, 426–434; (*g*) B. Dereka, A. Rosspeintner, R. Stężycki, C. Ruckebusch, D. T. Gryko and E. Vauthey, *J. Phys. Chem. Lett.*, 2017, 6029–6034; (*h*) B. Dereka and E. Vauthey, *J. Phys. Chem. Lett.*, 2017, **8**, 3927–3932; (*i*) Y. Li, M. Zhou, Y. Niu, Q. Guo and A. Xia, *J. Chem. Phys.*, 2015, **143**, 034309.

Open Access Article. Published on 20 November 2019. Downloaded on 1/17/2025 4:01:46 PM.
This article is licensed under a Creative Commons Attribution-NonCommercial 3.0 Unported Licence.

18 A. Aster, G. Licari, F. Zinna, E. Brun, T. Kumpulainen, E. Tajkhorshid, J. Lacour and E. Vauthey, *Chem. Sci.*, 2019, **10**, 10629–10639.

19 (*a*) Y. Sawada, S. Furumi, A. Takai, M. Takeuchi, K. Noguchi and K. Tanaka, *J. Am. Chem. Soc.*, 2012, **134**, 4080–4083; (*b*) P. Reine, A. G. Campaña, L. Alvarez de Cienfuegos, V. Blanco, S. Abbate, A. J. Mota, G. Longhi, D. Miguel and J. M. Cuerva, *Chem. Commun.*, 2019, **55**, 10685–10688; (*c*) C. Schaack, L. Arrico, E. Sidler, M. Gorecki, L. Di Bari and F. Diederich, *Chem.–Eur. J.*, 2019, **25**, 8003–8007; (*d*) K. Nakamura, S. Furumi, M. Takeuchi, T. Shibuya and K. Tanaka, *J. Am. Chem. Soc.*, 2014, **136**, 5555–5558; (*e*) Y. Hashimoto, T. Nakashima, D. Shimizu and T. Kawai, *Chem. Commun.*, 2016, **52**, 5171–5174; (*f*) S. Ito, K. Ikeda, S. Nakanishi, Y. Imai and M. Asami, *Chem. Commun.*, 2017, **53**, 6323–6326; (*g*) A. Homberg, E. Brun, F. Zinna, S. Pascal, M. Gorecki, L. Monnier, C. Besnard, G. Pescitelli, L. Di Bari and J. Lacour, *Chem. Sci.*, 2018, **9**, 7043–7052.

This journal is © The Royal Society of Chemistry 2020